IOPscience iopscience.iop.org

Home Search Collections Journals About Contact us My IOPscience

A simple 2D analytical threshold voltage model for fully depleted short-channel silicon-on-insulator MOSFETs

This content has been downloaded from IOPscience. Please scroll down to see the full text.

2004 Semicond. Sci. Technol. 19 1397

(http://iopscience.iop.org/0268-1242/19/12/012)

View the table of contents for this issue, or go to the journal homepage for more

Download details:

IP Address: 140.113.38.11
This content was downloaded on 26/04/2014 at 13:30

Please note that terms and conditions apply.

INSTITUTE OF PHYSICS PUBLISHING SEMICONDUCTOR SCIENCE AND TECHNOLOGY

Semicond. Sci. Technol. **19** (2004) 1397–1405 PII: S0268-1242(04)79212-3

A simple 2D analytical threshold voltage model for fully depleted short-channel silicon-on-insulator MOSFETs

Kow-Ming Chang and Han-Pang Wang

Department of Electronics Engineering, National Chiao-Tung University, Hsinchu, Taiwan 300, Republic of China

E-mail: kmchang@cc.nctu.edu.tw and u8911804@cc.nctu.edu.tw

Received 15 April 2004, in final form 5 August 2004
Published 3 November 2004
Online at stacks.iop.org/SST/19/1397
doi:10.1088/0268-1242/19/12/012

Abstract
In this paper, we propose a simple two-dimensional (2D) analytical threshold voltage model for deep-submicrometre fully depleted SOI MOSFETs using the three-zone Green's function technique to solve the 2D Poisson equation and adopting a new concept of the average electric field to avoid iterations in solving the position of the minimum surface potential. Firstly, we obtain the 2D potential distribution in the Si-film region by using the Green's function technique to solve the 2D Poisson equation. Then, by applying Gauss's law at the Si–SiO_2 interface, the initial expression of the threshold voltage is obtained. Eventually, we introduce a modified factor to compensate for the errors resulting from the charge-sharing effect in the derivations of the final threshold voltage model. The proposed model is validated against the results obtained by 2D numerical analysis and experimental data, and excellent agreements are obtained. The proposed model has an explicit expression and can be implemented into the circuit simulator.

Nomenclature

ε_{si} (ε_{ox})	the dielectric permittivity of Si (SiO_2)
q	the elementary charge
$\rho(x, y)$	the two-dimensional charge density
t_{si}	the thickness of silicon film
t_{fox} (t_{box})	the thickness of front (back) gate oxide
n_i	the intrinsic carrier concentration of Si semiconductor
$L(W)$	the effective channel length (width)
C_{fox} (C_{box})	the capacitance per unit area of the front (back) gate oxide
C_{si}	the capacitance per unit area of the silicon film
V_{GS} (V_{gs})	the external (intrinsic) gate–source voltage
V_{DS} (V_{ds})	the external (intrinsic) drain–source voltage
V_{BS} (V_{bs})	the external (intrinsic) back gate–source voltage
V_{FB}^{f} (V_{FB}^{b})	the flat band voltage of the front (back) gate
V'_{gs} (V'_{bs})	$V'_{gs} = V_{gs} - V_{FB}^{f}$ $\left(V'_{bs} = V_{bs} - V_{FB}^{b}\right)$
$V_{bi}(y)$	the built-in potential of the source (drain)/body junctions in zone II
$N_B f(y)$	the doping profile in zone II, where $f(y)$ is a doping profile function
N_D	the doping concentration in the source–drain region
k_n^i	the eigenvalue of zone i (i = I, II, III). $k_n^I = ((n-1/2)\pi)/t_{fox}$ for zone I, $k_n^{II} = n\pi/t_{si}$ for zone II and $k_n^{III} = ((n-1/2)\pi)/t_{box}$ for zone III
k_m	the eigenvalue in all zones $k_m = m\pi/L$
$D_{sf}(x)$ ($D_{sb}(x)$)	the electric displacement at the front (back) Si–SiO_2 interface
$\phi^i(x, y)$	the 2D potential distribution in zone i (i = I, II, III)
$E_y^i(x, y)$	the 2D vertical electric field distribution in zone i (i = I, II, III)
$\phi_{sf}^{II}(x)$ $\left(\phi_{sb}^{II}(x)\right)$	the front (back) surface potential in zone II

 © 2004 IOP Publishing Ltd Printed in the UK

$Q_B^n\ (Q_B^0)$ the Fourier coefficient of the bulk charge density with the integer $n (n = 0)$ in zone II:

$$Q_B^n = \frac{2}{t_{\mathrm{si}}}\int_0^{t_{\mathrm{si}}} (-qN_B f(y)) \cos k_n^{\mathrm{II}} y \cdot \mathrm{d}y$$

$$Q_B^0 = \frac{1}{t_{\mathrm{si}}}\int_0^{t_{\mathrm{si}}} (-qN_B f(y)) \cdot \mathrm{d}y$$

$D_{\mathrm{sf}}^m\ (D_{\mathrm{sb}}^m)$ the Fourier coefficient of the electric displacement at the front (back) surface:

$$D_{\mathrm{sf}}^m = \frac{2}{L}\int_0^L D_{\mathrm{sf}}(x) \sin(k_m x) \cdot \mathrm{d}x$$

$$D_{\mathrm{sb}}^m = \frac{2}{L}\int_0^L D_{\mathrm{sb}}(x) \sin(k_m x) \cdot \mathrm{d}x$$

$A_n^S\ (A_n^D)$ the Fourier coefficient of the boundary potential at the source (drain) side in zone I:

$$A_n^S = \frac{2}{t_{\mathrm{fox}}}\int_0^{t_{\mathrm{fox}}} \phi^{\mathrm{I}}(0, y) \cos k_n^{\mathrm{I}} y \cdot \mathrm{d}y$$

$$A_n^D = \frac{2}{t_{\mathrm{fox}}}\int_0^{t_{\mathrm{fox}}} \phi^{\mathrm{I}}(L, y) \cos k_n^{\mathrm{I}} y \cdot \mathrm{d}y$$

$B_n^S\ (B_0^S)$ the Fourier coefficient of the source boundary potential with the integer $n\ (n = 0)$ in zone II:

$$B_n^S = \frac{2}{t_{\mathrm{si}}}\int_0^{t_{\mathrm{si}}} V_{\mathrm{bi}}(y) \cos k_n^{\mathrm{II}} y \cdot \mathrm{d}y$$

$$B_0^S = \frac{1}{t_{\mathrm{si}}}\int_0^{t_{\mathrm{si}}} V_{\mathrm{bi}}(y) \cdot \mathrm{d}y$$

$B_n^D\ (B_0^D)$ the Fourier coefficient of the drain boundary potential with the integer $n\ (n = 0)$ in zone II:

$$B_n^D = \frac{2}{t_{\mathrm{si}}}\int_0^{t_{\mathrm{si}}} (V_{\mathrm{bi}}(y) + V_{\mathrm{ds}}) \cos k_n^{\mathrm{II}} y \cdot \mathrm{d}y$$

$$B_0^D = \frac{1}{t_{\mathrm{si}}}\int_0^{t_{\mathrm{si}}} (V_{\mathrm{bi}}(y) + V_{\mathrm{ds}}) \cdot \mathrm{d}y$$

$C_n^S\ (C_n^D)$ the Fourier coefficient of the boundary potential at the source (drain) side in zone III:

$$C_n^S = \frac{2}{t_{\mathrm{box}}}\int_0^{t_{\mathrm{box}}} \phi^{\mathrm{III}}(0, y) \cos k_n^{\mathrm{III}} y \cdot \mathrm{d}y$$

$$C_n^D = \frac{2}{t_{\mathrm{box}}}\int_0^{t_{\mathrm{box}}} \phi^{\mathrm{III}}(L, y) \cos k_n^{\mathrm{III}} y \cdot \mathrm{d}y$$

$\phi_{f,\mathrm{inv}}$ the front surface potential at the onset of strong inversion: $\phi_{f,\mathrm{inv}} = 2\phi_{\mathrm{fp}} = 2\left(\frac{k_B T}{q}\right)\ln\left(\frac{N_B}{n_i}\right)$

1. Introduction

Fully depleted (FD) silicon-on-insulator (SOI) CMOS technology is becoming another major technology for the next generation of VLSI [1–3]. This is because FD SOI CMOS transistors provide superior electrical characteristics over bulk CMOS devices [4–6] such as reduced source–drain junction capacitances [7], increased carrier mobility [8], suppressed short channel effect [9], improved subthreshold slope [10], improved latch-up immunity [11] and better radiation hardness [12]. However, the coupling effect between the front gate and back gate becomes complicated, especially for short channel devices. Therefore, it is difficult to develop a simple and accurate analytical model for circuit design and device characterization.

In general, the threshold voltage of a MOS transistor is a very important physical parameter in the device design. On the other hand, the accuracy of the threshold voltage model plays a more important role in the device optimization and circuit design. The analytical modelling of the threshold voltage of the FD SOI MOS transistor has already been proposed by numerous authors [13–16]. In a paper by Young [13], the potential distribution in the Si film was approximated by a simple parabolic function. This simplified assumption underestimates the coupling effect of the source–drain region and may cause a significant error in the prediction of threshold voltage when the channel length continues to scale down. In a paper by Veeraraghavan and Fossum [14], the threshold voltage model was developed based on the conventional charge-sharing scheme and it predicted a $1/L_{\mathrm{eff}}$ dependent threshold voltage shift. In the range of submicrometre channel length, the assumption of constant surface potential of the charge-sharing model is invalid. In a paper by Woo *et al* [15], the work was done by decomposition of the 2D Poisson equation into a 1D Poisson equation and a 2D Laplace equation. In a paper by Guo and Wu [16], an accurate 2D analytical threshold voltage model was developed by means of the three-zone Green's function solution technique. Although an explicit form of the threshold voltage is derived, the calculation is too complicated to be further implemented in the derivation of the *I–V* model for a simulator such as SPICE. Therefore, to consider an efficient computation, the simplified and explicit expression of the threshold voltage of the FD SOI MOS transistor is necessary.

In this paper, in order to derive the threshold voltage model, the three-zone Green's function technique [16] is used to solve the 2D Poisson equation. Based on the concept of the average vertical electric field, a simple and explicit expression of the threshold voltage is obtained and described in section 2. Comparisons between the 2D numerical analysis, experiments and the proposed analytical threshold voltage model are shown in section 3. Finally, the conclusions are summarized in section 4.

2. Derivation of the analytical threshold voltage model

2.1. The basic analysis

The conventional structure of an FD SOI MOS transistor for 2D numerical simulation is presented in figure 1. A simplified domain has been used for solving the 2D Poisson equation and indicated by the bold lines in figure 1. The domain for solving the 2D Poisson equation is further divided into three sub-domains (zones I, II and III) to avoid the complexity of calculating the equivalent charge density between the regions with different dielectrics. Zone I is the front gate oxide,

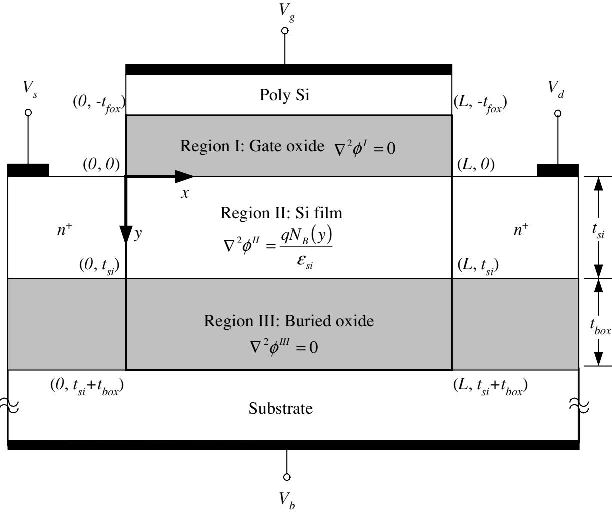

Figure 1. Schematic diagram of a fully depleted SOI MOSFET, where the simplified domains for analytically solving the 2D Poisson equation are indicated by the bold lines.

Table 1. List of the boundary conditions relating to the fully depleted SOI MOSFET shown in figure 1.

Zone	Boundary conditions
Zone I :	$\phi^{\mathrm{I}}(L, y) = V_{\mathrm{bi}}(0) + V_{\mathrm{ds}} + \frac{V_{\mathrm{bi}}(0)+V_{\mathrm{ds}}-V'_{\mathrm{gs}}}{t_{\mathrm{fox}}} y$
	$\phi^{\mathrm{I}}(0, y) = V_{\mathrm{bi}}(0) + \frac{V_{\mathrm{bi}}(0)-V'_{\mathrm{gs}}}{t_{\mathrm{fox}}} y$
	$\phi^{\mathrm{I}}(x, -t_{\mathrm{fox}}) = V_{\mathrm{gs}} - V_{\mathrm{fb},f} = V'_{\mathrm{gs}}$
	$D_{\mathrm{sf}}(x, 0) = \varepsilon_{\mathrm{ox}} E_y^{\mathrm{I}}(x, 0)$
Zone II :	$\phi^{\mathrm{II}}(L, y) = V_{\mathrm{bi}}(y) + V_{\mathrm{ds}}$
	$\phi^{\mathrm{II}}(0, y) = V_{\mathrm{bi}}(y)$
	$D_{\mathrm{sf}}(x, 0) = \varepsilon_{\mathrm{si}} E_y^{\mathrm{II}}(x, 0)$
	$D_{\mathrm{sb}}(x, t_{\mathrm{si}}) = \varepsilon_{\mathrm{si}} E_y^{\mathrm{II}}(x, t_{\mathrm{si}})$
Zone III :	$\phi^{\mathrm{III}}(L, y) = V_{\mathrm{bi}}(t_{\mathrm{si}}) + V_{\mathrm{ds}} - \frac{V_{\mathrm{bi}}(t_{\mathrm{si}})+V_{\mathrm{ds}}-V'_{\mathrm{bs}}}{t_{\mathrm{box}}}(y - t_{\mathrm{si}})$
	$\phi^{\mathrm{III}}(0, y) = V_{\mathrm{bi}}(t_{\mathrm{si}}) - \frac{V_{\mathrm{bi}}(t_{\mathrm{si}})-V'_{\mathrm{bs}}}{t_{\mathrm{box}}}(y - t_{\mathrm{si}})$
	$\phi^{\mathrm{III}}(x, t_{\mathrm{si}} + t_{\mathrm{box}}) = V_{\mathrm{bs}} - V_{\mathrm{fb},b} = V'_{\mathrm{bs}}$
	$D_{\mathrm{sb}}(x, t_{\mathrm{si}}) = \varepsilon_{\mathrm{ox}} E_y^{\mathrm{III}}(x, t_{\mathrm{si}})$

zone II represents the Si film and zone III is the buried oxide. The boundary conditions used for each zone are enumerated in table 1. It should be noted that the boundary potential in the y-direction in zones I and III is assumed to vary linearly [15].

Based on the assumption that the front gate oxide and buried oxide are well grown and no charge resides there, the 2D Poisson equations in zones I and III can be reduced to two 2D Laplace equations. Substituting the Green's function solutions, listed in table 2, into Green's theorem [17], which is given as

$$\phi(x, y) = \int\!\!\int \frac{\rho(x', y')}{\varepsilon} G(x, y : x', y')\,\mathrm{d}x'\,\mathrm{d}y' + \int G(x, y : x', y') \frac{\partial \phi}{\partial n'}\,\mathrm{d}S' - \int \phi(x', y') \frac{\partial G}{\partial n'}\,\mathrm{d}S', \quad (1)$$

where $G(x, y : x', y')$ is the Green's function satisfying $\nabla^2 G = -\delta(x - x')\delta(y - y')$, n' is the outward normal direction on the boundary surface, and neglecting the free carriers, the general form of the 2D potential distribution in each zone can be obtained as follows [16]:

$$\begin{aligned}\phi^{\mathrm{I}}(x, y) = {} & \sum_{m=\mathrm{odd}}^{\infty} \frac{4V'_{\mathrm{gs}}}{m\pi} \frac{\cosh k_m y}{\cosh k_m t_{\mathrm{fox}}} \sin k_m x - \sum_{m=1}^{\infty} \frac{D_{\mathrm{sf}}^m}{\varepsilon_{\mathrm{ox}}} \frac{\sinh k_m (t_{\mathrm{fox}} + y)}{k_m \cosh k_m t_{\mathrm{fox}}} \sin k_m x \\ & + \sum_{n=1}^{\infty} \frac{\cos k_n^{\mathrm{I}} y}{\sin k_n^{\mathrm{I}} L} \left[A_n^S \sinh k_n^{\mathrm{I}}(L - x) + A_n^D \sinh k_n^{\mathrm{I}} x\right], \end{aligned} \quad (2)$$

$$\begin{aligned}\phi^{\mathrm{II}}(x, y) = {} & \frac{Q_B^0}{2\varepsilon_{\mathrm{si}}} x(L - x) + \sum_{n=1}^{\infty} \frac{Q_B^n}{\varepsilon_{\mathrm{si}}} \frac{\cos k_n^{\mathrm{II}} y}{\left(k_n^{\mathrm{II}}\right)^2} \times \left[1 \frac{\sinh k_n^{\mathrm{II}} x + \sinh k_n^{\mathrm{II}}(L - x)}{\sinh k_n^{\mathrm{II}} L}\right] + B_0^s \left(1 - \frac{x}{L}\right) \\ & + B_0^D \frac{x}{L} + \sum_{n=1}^{\infty} \frac{\cos k_n^{\mathrm{II}} y}{\sinh k_n^{\mathrm{II}} L} \times \left[B_n^S \sinh k_n^{\mathrm{II}}(L - x) + B_n^D \sinh k_n^{\mathrm{II}} x\right] \\ & + \sum_{m=1}^{\infty} \frac{\sin k_m x}{\varepsilon_{\mathrm{si}}\, k_m \sinh k_m t_{\mathrm{si}}} \times \left[D_{\mathrm{sf}}^m \cosh k_m (t_{\mathrm{si}} - y) - D_{\mathrm{sb}}^m \cosh k_m y\right], \end{aligned} \quad (3)$$

$$\begin{aligned}\phi^{\mathrm{III}}(x, y) = {} & \sum_{m=\mathrm{odd}}^{\infty} \frac{4V_{\mathrm{bs}}}{m\pi} \frac{\cosh k_m (y - t_{\mathrm{si}})}{\cosh k_m t_{\mathrm{box}}} \sin k_m x + \sum_{m=1}^{\infty} \frac{D_{\mathrm{sb}}^m}{\varepsilon_{\mathrm{ox}}} \frac{\sinh k_m (t_{\mathrm{box}} + t_{\mathrm{si}} - y)}{k_m \cosh k_m t_{\mathrm{box}}} \sin k_m x \\ & + \sum_{n=1}^{\infty} \frac{\cos k_n^{\mathrm{III}} (y - t_{\mathrm{si}})}{\sin k_n^{\mathrm{III}} L} \times \left[C_n^s \sinh k_n^{\mathrm{III}} (L - x) + C_n^D \sinh k_n^{\mathrm{III}} x\right], \end{aligned} \quad (4)$$

where the definitions of the Fourier coefficients A_n^s, A_n^d, B_0^S, B_0^D, B_n^S, B_n^D, C_n^S, C_n^D, D_{sf}^m, D_{sb}^m, Q_B^0 and Q_B^n are given in the nomenclature. In order to obtain the 2D analytical solution of the potential distribution at zone II, first D_{sf}^m and D_{sb}^m must be solved. D_{sf}^m and D_{sb}^m can be obtained by equating equations (2) and (3) at $y = 0$ and equations (3) and (4) at $y = t_{\mathrm{si}}$. The related expressions are given in table 3. It should be noted that the above equations are exact in the sense that any arbitrary doping profile in the Si film can be treated. In the following analysis, uniformly doped Si film is assumed for simplicity. Therefore, the 2D potential distribution at zone II can be further reexpressed as follows [16]:

$$\begin{aligned}\phi^{\mathrm{II}}(x, y) = {} & -\frac{qN_B}{2\varepsilon_{\mathrm{si}}} x(L - x) + \sum_{m=1}^{\infty} \frac{\sin k_m x}{\varepsilon_{\mathrm{si}} k_m \sinh k_m t_{\mathrm{si}}} \\ & \times \left[D_{\mathrm{sf}}^m \cosh k_m (t_{\mathrm{si}} - y) - D_{\mathrm{sb}}^m \cosh k_m y\right] + V_{\mathrm{bi}} + \frac{x}{L} V_{\mathrm{ds}}. \end{aligned} \quad (5)$$

2.2. *A new approach for the development of the threshold voltage model*

Since the FD SOI MOS transistor under consideration is normally-off type (enhancement mode), the front surface

Table 2. The solution of Green's function for zones I, II and III.

$$\text{Zone I}: \begin{cases} G_x^{\mathrm{I}}(x, y; x', y') = \frac{2}{L}\sum_{m=1}^{\infty} \sin k_m x \sin k_m x' \frac{\cos k_m y \sinh k_m (t_{\mathrm{fox}}+y')}{k_m \cosh k_m t_{\mathrm{fox}}}, & y' < y \\ G_x^{\mathrm{I}}(x, y; x', y') = \frac{2}{L}\sum_{m=1}^{\infty} \sin k_m x \sin k_m x' \frac{\cos k_m y' \sinh k_m (t_{\mathrm{fox}}+y)}{k_m \cosh k_m t_{\mathrm{fox}}}, & y < y' \\ G_y^{\mathrm{I}}(x, y; x', y') = \frac{2}{t_{\mathrm{fox}}}\sum_{n=1}^{\infty} \cos k_n^{\mathrm{I}} y \cos k_n^{\mathrm{I}} y' \frac{\sinh k_n^{\mathrm{I}} x \sinh k_n^{\mathrm{I}} (L-x')}{k_n^{\mathrm{I}} \sinh k_n^{\mathrm{I}} L}, & x < x' \\ G_y^{\mathrm{I}}(x, y; x', y') = \frac{2}{t_{\mathrm{fox}}}\sum_{n=1}^{\infty} \cos k_n^{\mathrm{I}} y \cos k_n^{\mathrm{I}} y' \frac{\sinh k_n^{\mathrm{I}} x' \sinh k_n^{\mathrm{I}} (L-x)}{k_n^{\mathrm{I}} \sinh k_n^{\mathrm{I}} L}, & x' < x \end{cases}$$

$$\text{Zone II}: \begin{cases} G_x^{\mathrm{II}}(x, y; x', y') = \frac{2}{L}\sum_{m=1}^{\infty} \sin k_m x \sin k_m x' \frac{\cos k_m y \cosh k_m (t_{\mathrm{si}}-y')}{k_m \sinh k_m t_{\mathrm{si}}}, & y' < y \\ G_x^{\mathrm{II}}(x, y; x', y') = \frac{2}{L}\sum_{m=1}^{\infty} \sin k_m x \sin k_m x' \frac{\cos k_m y' \cosh k_m (t_{\mathrm{si}}-y)}{k_m \cosh k_m t_{\mathrm{fox}}}, & y < y' \\ G_y^{\mathrm{II}}(x, y; x', y') = \frac{c}{t_{\mathrm{si}}}\sum_{n=1}^{\infty} \cos k_n^{\mathrm{II}} y \cos k_n^{\mathrm{II}} y' \frac{\sinh k_n^{\mathrm{II}} x \sinh k_n^{\mathrm{II}} (L-x')}{k_n^{\mathrm{II}} \sinh k_n^{\mathrm{II}} L}, & x < x' \\ G_y^{\mathrm{II}}(x, y; x', y') = \frac{c}{t_{\mathrm{si}}}\sum_{n=1}^{\infty} \cos k_n^{\mathrm{II}} y \cos k_n^{\mathrm{II}} y' \frac{\sinh k_n^{\mathrm{II}} x' \sinh k_n^{\mathrm{II}} (L-x)}{k_n^{\mathrm{II}} \sinh k_n^{\mathrm{II}} L}, & x' < x \end{cases}$$

$c = 1$ for $n = 0$; $c = 2$ for $n > 0$.

$$\text{Zone III}: \begin{cases} G_x^{\mathrm{III}}(x, y; x', y') = \frac{2}{L}\sum_{m=1}^{\infty} \sin k_m x \sin k_m x' \frac{\cos k_m (y-t_{\mathrm{si}}) \sinh k_m (t_{\mathrm{box}}+t_{\mathrm{si}}-y')}{k_m \cosh k_m t_{\mathrm{box}}}, & y' < y \\ G_x^{\mathrm{III}}(x, y; x', y') = \frac{2}{L}\sum_{m=1}^{\infty} \sin k_m x \sin k_m x' \frac{\cos k_m (y'-t_{\mathrm{si}}) \sinh k_m (t_{\mathrm{box}}+t_{\mathrm{si}}-y)}{k_m \cosh k_m t_{\mathrm{box}}}, & y < y' \\ G_y^{\mathrm{III}}(x, y; x', y') = \frac{2}{t_{\mathrm{box}}}\sum_{n=1}^{\infty} \cos k_n^{\mathrm{III}} (y - t_{\mathrm{si}}) \cos k_n^{\mathrm{III}} (y' - t_{\mathrm{si}}) \frac{\sinh k_n^{\mathrm{III}} x \sinh k_n^{\mathrm{III}} (L-x')}{k_n^{\mathrm{III}} \sinh k_n^{\mathrm{III}} L}, & x < x' \\ G_y^{\mathrm{III}}(x, y; x', y') = \frac{2}{t_{\mathrm{box}}}\sum_{n=1}^{\infty} \cos k_n^{\mathrm{III}} (y - t_{\mathrm{si}}) \cos k_n^{\mathrm{III}} (y' - t_{\mathrm{si}}) \frac{\sinh k_n^{\mathrm{III}} x' \sinh k_n^{\mathrm{III}} (L-x)}{k_n^{\mathrm{III}} \sinh k_n^{\mathrm{III}} L}, & x' < x \end{cases}$$

Table 3. The expressions of the Fourier coefficients D_{sf}^m, D_{sb}^m and related parameters.

$$D_{\mathrm{sf}}^m = \frac{\varepsilon_{\mathrm{si}} k_m}{d_0^m}\left[\frac{d_2^m}{\sinh(k_m t_{\mathrm{si}})} - d_1^m\left(\frac{1}{\tanh(k_m t_{\mathrm{si}})} + \frac{\varepsilon_{\mathrm{si}}}{\varepsilon_{\mathrm{ox}}}\tanh(k_m t_{\mathrm{box}})\right)\right]$$

$$D_{\mathrm{sb}}^m = \frac{\varepsilon_{\mathrm{si}} k_m}{d_0^m}\left[-\frac{d_1^m}{\sinh(k_m t_{\mathrm{si}})} + d_2^m\left(\frac{1}{\tanh(k_m t_{\mathrm{si}})} + \frac{\varepsilon_{\mathrm{si}}}{\varepsilon_{\mathrm{ox}}}\tanh(k_m t_{\mathrm{fox}})\right)\right]$$

$$d_0^m = \frac{1}{[\sinh(k_m t_{\mathrm{si}})]^2} - \left(\frac{1}{\tanh(k_m t_{\mathrm{si}})} + \frac{\varepsilon_{\mathrm{si}}}{\varepsilon_{\mathrm{ox}}}\tanh(k_m t_{\mathrm{fox}})\right)\left(\frac{1}{\tanh(k_m t_{\mathrm{si}})} + \frac{\varepsilon_{\mathrm{si}}}{\varepsilon_{\mathrm{ox}}}\tanh(k_m t_{\mathrm{box}})\right)$$

$$d_1^m = -\phi_q^m + \left(\frac{2V_{\mathrm{gs}}'}{m\pi}\right)\left(\frac{1-(-1)^m}{\cosh(k_m t_{\mathrm{fox}})}\right) + h_m^{\mathrm{I}}$$

$$d_2^m = -\phi_q^m + \left(\frac{2V_{\mathrm{bs}}'}{m\pi}\right)\left(\frac{1-(-1)^m}{\cosh(k_m t_{\mathrm{box}})}\right) + h_m^{\mathrm{III}}$$

$$h_m^{\mathrm{I}} = \sum_{n=1}^{\infty}\frac{1}{2} t_{mn}^{\mathrm{I}}\left[A_n^S + (-1)^{m+1} A_n^D\right]$$

$$h_m^{\mathrm{III}} = \sum_{n=1}^{\infty}\frac{1}{2} t_{mn}^{\mathrm{III}}\left[C_n^S + (-1)^{m+1} C_n^D\right]$$

$$t_{mn}^{\mathrm{I}} = \frac{4}{m\pi}\left[1 + \frac{L^2(n-0.5)^2}{t_{\mathrm{fox}}^2 m^2}\right]^{-1}$$

$$t_{mn}^{\mathrm{III}} = \frac{4}{m\pi}\left[1 + \frac{L^2(n-0.5)^2}{t_{\mathrm{box}}^2 m^2}\right]^{-1}$$

$$\phi_q^m = \frac{2}{m\pi}\left[(1-(-1)^m)\left(-\frac{qN_B}{\varepsilon_{\mathrm{si}}}\frac{L^2}{(m\pi)^2}\right) + (1-(-1)^m)V_{\mathrm{bi}} + (-1)^{m+1}V_{\mathrm{ds}}\right]$$

potential distribution of the Si film is usually used to monitor the turn-on status of FD SOI MOSFETs. From equation (5), the potential distribution along the front surface of the Si film can be derived as

$$\phi^{\mathrm{II}}(x, 0) = -\frac{qN_B}{2\varepsilon_{\mathrm{si}}} x(L - x) + \sum_{m=1}^{\infty}\frac{\sin k_m x}{\varepsilon_{\mathrm{si}} k_m \sinh k_m t_{\mathrm{si}}} \times \left[D_{\mathrm{sf}}^m \cosh k_m t_{\mathrm{si}} - D_{\mathrm{sb}}^m\right] + V_{\mathrm{bi}} + \frac{x}{L}V_{\mathrm{ds}}. \quad (6)$$

The accuracy of the derived front surface potential distribution in the Si film has been verified by 2D numerical analysis as shown in [16]. In the paper by Guo [16], to develop an analytical threshold voltage model, the minimum potential along the front surface of the Si film has to be calculated first. By differentiating equation (6), the position of the minimum potential along the front surface of the Si film can be calculated,

$$\left.\frac{\partial\phi^{\mathrm{II}}(x, 0)}{\partial x}\right|_{x=x_{\mathrm{mim}}} = \left.\frac{\partial\phi_{\mathrm{sf}}^{\mathrm{II}}(x)}{\partial x}\right|_{x=x_{\mathrm{mim}}} = 0, \quad (7)$$

where x_{min} is the position of the minimum surface potential and $\phi_{\mathrm{sf}}^{\mathrm{II}}(x)$ represents the potential distribution along the front surface of the Si film. By introducing the value of x_{min} into equation (6), the minimum surface potential $\phi_{\mathrm{sf,min}}^{\mathrm{II}}$ can be obtained. However, the position of the minimum surface potential x_{min} can only be solved iteratively and no explicit form of x_{min} can be obtained. Therefore, calculation of the minimum front surface potential is too complicated to be further implemented in the derivations of the analytical *I–V* model for a circuit simulator such as SPICE.

A new approach for development of the threshold voltage model is described in the following. Firstly, by differentiating equation (3) with respect to y, the normal electric field along the front Si-film surface can be obtained and expressed as

$$E_{\mathrm{sf}}(x) = -\left.\frac{\partial\phi^{\mathrm{II}}(x, y)}{\partial y}\right|_{y=0} = \sum_{m=1}^{\infty}\frac{D_{\mathrm{sf}}^m}{\varepsilon_{\mathrm{si}}}\sin k_m x. \quad (8)$$

Then, by integrating equation (8) with respect to x from $x = 0$ to $x = L$, the total charge density controlled by the front gate can be obtained and expressed as

$$Q_{\mathrm{fg}} = -\int_0^L \varepsilon_{\mathrm{si}} E_{\mathrm{sf}}(x)\,\mathrm{d}x = -\sum_{m=1}^{\infty} \frac{D_{\mathrm{sf}}^m}{k_m}[1-(-1)^m]. \quad (9)$$

By applying Gauss's law at the front SiO_2–Si interface, we obtain

$$E_{\mathrm{sf}}(x) = \frac{C_{\mathrm{fox}}\left(V_{\mathrm{gs}} - V_{\mathrm{FB}}^f - \phi_{\mathrm{sf}}^{\mathrm{II}}(x)\right)}{\varepsilon_{\mathrm{si}}}. \quad (10)$$

From equation (10), the threshold voltage can be obtained as

$$V_{\mathrm{TH}} = V_{\mathrm{FB}}^f + \phi_{f,\mathrm{inv}} + \frac{\varepsilon_{\mathrm{si}} E_{\mathrm{sf}}(x_{\min})}{C_{\mathrm{fox}}}, \quad (11)$$

where the threshold voltage is defined as the value of gate voltage V_{gs} for which $\phi_{\mathrm{sf,min}}^{\mathrm{II}} = \phi_{f,\mathrm{inv}} = 2\phi_{\mathrm{fp}}$. However, the derivation of equation (11) is still complicated and computationally inefficient due to the calculation of $x_{\min}$. Therefore, in this work, the average normal electric field along the front surface of the Si film $\overline{E_{\mathrm{sf}}}$ is used to substitute the $E_{\mathrm{sf}}(x_{\min})$. From equation (9), $\overline{E_{\mathrm{sf}}}$ can be obtained and expressed as

$$\overline{E_{\mathrm{sf}}} = \sum_{m=1}^{\infty} \frac{D_{\mathrm{sf}}^m}{\varepsilon_{\mathrm{si}} k_m L}[1-(-1)^m]. \quad (12)$$

Then, the threshold voltage can be redefined as

$$V_{\mathrm{TH}} = V_{\mathrm{FB}}^f + \phi_{f,\mathrm{inv}} + \frac{\varepsilon_{\mathrm{si}} \overline{E_{\mathrm{sf}}}}{C_{\mathrm{fox}}}. \quad (13)$$

Due to the effect of the lateral electric field originating from the source–drain junctions, the average normal electric field along the front surface of the Si film is expected to be smaller than the normal electric field at the position of minimum potential. Therefore, in order to compensate the error results from the charge-sharing effect, a modification to equation (13) is necessary.

Figure 2 shows the normal electric field along the front SiO_2–Si interface of the FD SOI MOSFETs, where the case of the average surface normal electric field is shown in (*a*) and the case of the surface normal electric field accounting for the charge-sharing effect is shown in (*b*). In figure 2(*a*), the total depletion charges $Q_{\mathrm{depl},1}$ in the Si film that terminate the average surface normal electric field originating from the gate can be expressed as

$$Q_{\mathrm{depl},1} = \varepsilon_{\mathrm{si}} \overline{E_{\mathrm{sf}}} W L t_{\mathrm{si}}. \quad (14)$$

The charge-sharing effect is due to the loss of control ability of the gate over the depletion charge under it. In other words, the depletion charge controlled by the gate is no longer equal to $Q_{\mathrm{depl,bulk}}$ ($Q_{\mathrm{depl,bulk}} = qN_B y_{d\max}$, for bulk MOSFETs, where $y_{d\max}$ is the maximum depletion width of the depletion region under the gate), but to a fraction of it. The reduction of the depletion charge is due to the presence of the source–drain junctions and the surface normal electric field is disturbed by the lateral electric field originating from the source–drain junctions, as shown in figure 2(*b*). According to the charge-sharing scheme shown in figure 2(*b*), the effective depletion charge controlled by the gate can be obtained as

$$\begin{aligned} Q_{\mathrm{depl},2} &= W\left(\int_0^L \varepsilon_{\mathrm{si}} E_{\mathrm{sf}}(x)\,\mathrm{d}x\right)\frac{t_{\mathrm{si}}}{2L}(2L - \Delta L_1 - \Delta L_2) \\ &= W Q_{\mathrm{fg}} \frac{t_{\mathrm{si}}}{2L}(2L - \Delta L_1 - \Delta L_2) \end{aligned} \quad (15)$$

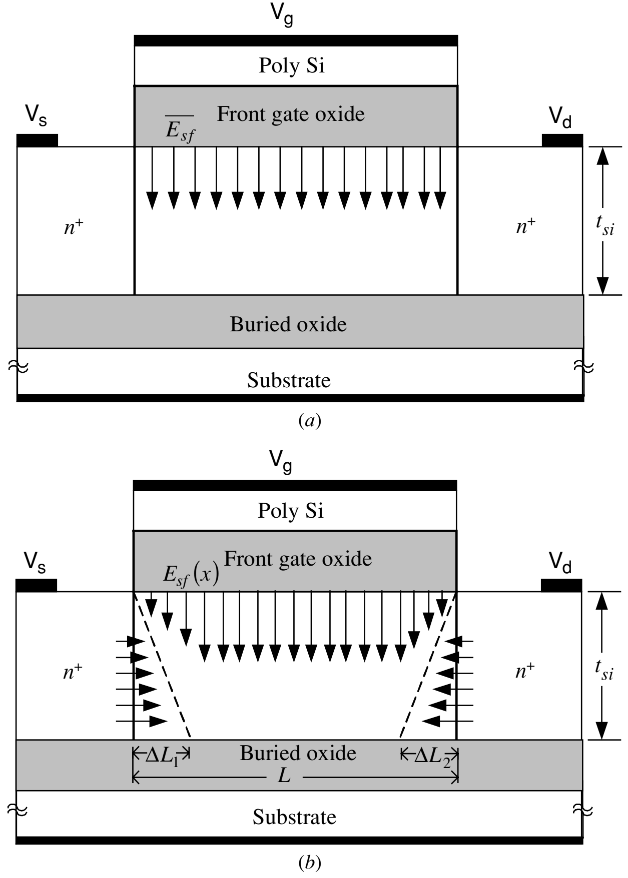

Figure 2. Schematic diagram of a fully depleted SOI MOSFET, where the arrows in (*a*) represent the average surface normal electric field and the arrows in (*b*) represent the surface normal electric field and lateral field originating from source–drain junctions.

where

$$\Delta L_1 \approx W_s = \left[\frac{2\varepsilon_{\mathrm{si}}(V_{\mathrm{bi}} - \phi_{f,\mathrm{inv}})}{qN_B}\right]^{1/2},$$

$$\Delta L_2 \approx W_d = \left[\frac{2\varepsilon_{\mathrm{si}}(V_{\mathrm{bi}} + V_{\mathrm{ds}} - \phi_{f,\mathrm{inv}})}{qN_B}\right]^{1/2},$$

where W_s and W_d are the depletion widths of the source- and drain-substrate junctions at the surface.

By equating equations (14) and (15), the relationship between Q_{fg} and $\overline{E_{\mathrm{sf}}}$ can be obtained as

$$Q_{\mathrm{fg}} = \varepsilon_{\mathrm{si}} \overline{E_{\mathrm{sf}}} \beta, \quad (16)$$

where

$$\beta = \frac{2L^2}{2L - \Delta L_1 - \Delta L_2} = L\left\{1 - \frac{\Delta L_1 + \Delta L_2}{2L}\right\}^{-1}.$$

Therefore, in order to compensate for the errors caused by the charge-sharing effect, we add the modified factor β into equation (13) and obtain the final expression of the analytical threshold voltage model:

$$V_{\mathrm{TH}} = V_{\mathrm{FB}}^f + \phi_{f,\mathrm{inv}} + \frac{\varepsilon_{\mathrm{si}} \overline{E_{\mathrm{sf}}}}{C_{\mathrm{fox}}}\beta. \quad (17)$$

Table 4. Expressions for the coefficients G^m, F_b^m, F_d^m and F_g^m.

$$G^m = \left[\frac{P_2^m}{\sinh(k_m t_{\rm si})} - P_1^m\left(\frac{1}{\tanh(k_m t_{\rm si})} + \frac{\varepsilon_{\rm si}}{\varepsilon_{\rm ox}}\tanh(k_m t_{\rm box})\right)\right]$$

$$F_g^m = -\left[\frac{1}{\tanh(k_m t_{\rm si})} + \frac{\varepsilon_{\rm si}}{\varepsilon_{\rm ox}}\tanh(k_m t_{\rm box})\right]\left[P_3^m + \frac{2}{m\pi}\frac{1-(-1)^m}{\cosh(k_m t_{\rm fox})}\right]$$

$$F_b^m = \frac{1}{\sinh(k_m t_{\rm si})}\left[P_4^m + \frac{2}{m\pi}\frac{1-(-1)^m}{\cosh(k_m t_{\rm box})}\right]$$

$$F_d^m = \left[\frac{P_5^m}{\sinh(k_m t_{\rm si})} - P_6^m\left(\frac{1}{\tanh(k_m t_{\rm si})} + \frac{\varepsilon_{\rm si}}{\varepsilon_{\rm ox}}\tanh(k_m t_{\rm box})\right)\right]$$

$$P_1^m = -\frac{2}{m\pi}[1-(-1)^m]\left(V_{\rm bi} - \frac{qN_B}{\varepsilon_{\rm si}}\frac{L^2}{(m\pi)^2}\right) + \sum_{n=1}^{\infty}\frac{t_{mn}^{\rm I}}{t_{\rm fox}k_{mn}^{\rm I}}[1-(-1)^{m+1}]\left[V_{\rm bi}\sin\left(n-\tfrac{1}{2}\right)\pi - \frac{V_{\rm bi}}{t_{\rm fox}}\left(t_{\rm fox}\sin\left(n-\tfrac{1}{2}\right)\pi\right) - \frac{1}{k_n^{\rm I}}\right]$$

$$P_2^m = -\frac{2}{m\pi}[1-(-1)^m]\left(V_{\rm bi} - \frac{qN_B}{\varepsilon_{\rm si}}\frac{L^2}{(m\pi)^2}\right) + \sum_{n=1}^{\infty}\frac{t_{mn}^{\rm III}}{t_{\rm box}k_{mn}^{\rm III}}[1-(-1)^{m+1}]\left[V_{\rm bi}\sin\left(n-\tfrac{1}{2}\right)\pi - \frac{V_{\rm bi}}{t_{\rm box}}\left(t_{\rm box}\sin\left(n-\tfrac{1}{2}\right)\pi\right) - \frac{1}{k_n^{\rm III}}\right]$$

$$P_3^m = \sum_{n=1}^{\infty}\frac{t_{mn}^{\rm I}}{t_{\rm fox}^2 k_n^{\rm I}}[1-(-1)^{m+1}]\left(t_{\rm fox}\sin\left(n-\tfrac{1}{2}\right)\pi - \frac{1}{k_n^{\rm I}}\right)$$

$$P_4^m = \sum_{n=1}^{\infty}\frac{t_{mn}^{\rm III}}{t_{\rm box}^2 k_n^{\rm III}}[1-(-1)^{m+1}]\left(t_{\rm box}\sin\left(n-\tfrac{1}{2}\right)\pi - \frac{1}{k_n^{\rm III}}\right)$$

$$P_5^m = \sum_{n=1}^{\infty}\frac{t_{mn}^{\rm III}}{t_{\rm box}k_n^{\rm III}}(-1)^{m+1}\left[\sin\left(n-\tfrac{1}{2}\right)\pi - \frac{1}{t_{\rm box}}\left(t_{\rm box}\sin\left(n-\tfrac{1}{2}\right)\pi - \frac{1}{k_n^{\rm III}}\right)\right] - \frac{2}{m\pi}(-1)^{m+1}$$

$$P_6^m = \sum_{n=1}^{\infty}\frac{t_{mn}^{\rm I}}{t_{\rm fox}k_n^{\rm I}}(-1)^{m+1}\left[\sin\left(n-\tfrac{1}{2}\right)\pi - \frac{1}{t_{\rm fox}}\left(t_{\rm fox}\sin\left(n-\tfrac{1}{2}\right)\pi - \frac{1}{k_n^{\rm I}}\right)\right] - \frac{2}{m\pi}(-1)^{m+1}$$

After some mathematical manipulations, equation (17) can be further expressed in terms of the terminal voltage as

$$V_{\rm TH} = V_{\rm FB}^f + X\left\{\phi_{f,{\rm inv}} + \frac{\varepsilon_{\rm si}\beta}{C_{\rm fox}}\sum_{m=1}^{\infty}\frac{1}{d_0^m}[1-(-1)^m] \times \left(G^m + F_b^m V_{\rm bs}' + \gamma F_d^m V_{\rm ds}\right)\right\}, \tag{18}$$

$$X = \left\{1 - \frac{\varepsilon_{\rm si}\beta}{C_{\rm fox}}\sum_{m=1}^{\infty}\frac{1}{d_0^m}F_g^m[1-(-1)^m]\right\}^{-1},$$

where the coefficients G^m, F_b^m, F_d^m and F_g^m are listed in table 4 and γ is an empirical constant assumed to account for the errors resulting from the drain-induced barrier lowering effect.

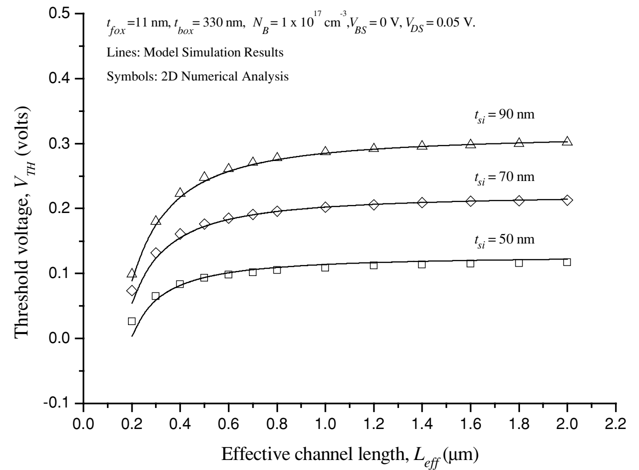

Figure 3. The calculated threshold voltage as a function of effective channel length with the thickness of the Si film as a parameter.

3. Model verifications

In order to verify the accuracy of the derived equations, the analytical model of the $V_{\rm TH}$, given in equation (18), has been compared with the results obtained by the 2D numerical device simulator Medici [18] and experimental data [19]. The threshold voltages of the results obtained by the 2D numerical simulator are defined by the relationship between the drain current and external gate–source voltage as follows. In general, the drain current in the *non-saturation* region can be expressed as

$$I_{\rm DS} = \frac{W_{\rm eff}C_{\rm fox}\mu_{\rm eff}}{L_{\rm eff}}\left(V_{\rm GS} - V_{\rm TH} - \frac{1}{2}V_{\rm DS}\right)V_{\rm DS}. \tag{19}$$

For the long channel length devices operating at low $V_{\rm DS}$ (e.g., $V_{\rm DS} = 50$ mV), using the extrapolation method on the $I_{\rm DS}$–$V_{\rm GS}$ curve at $V_{\rm GS}$ equal to the voltage at which the maximum $dI_{\rm DS}/dV_{\rm GS}$ occurs, the threshold voltage can be obtained by the intercept on the $V_{\rm GS}$-axis:

$$V_{\rm TH} = V_{\rm GS,intercept} - \tfrac{1}{2}V_{\rm DS}. \tag{20}$$

Additionally, when $V_{\rm GS} = V_{\rm TH}$, the normalized drain current is defined as a reference current,

$$I_{\rm reference} = I_{\rm DS,normalized} = \frac{L_{\rm eff}}{W_{\rm eff}}I_{\rm DS,longL} \tag{21}$$

where $I_{\rm reference}$ is the reference current, $I_{\rm DS,normalized}$ is the normalized drain current and $I_{\rm DS,longL}$ is the drain current of the long channel device. When the channel length is very short, the maximum transconductance extrapolation method would fail due to the significant short channel effect. Thus, the threshold voltage of the short channel device is extracted by equating the normalized drain current to the reference current, which is determined by the long channel device. For high $V_{\rm DS}$ operation, $V_{\rm TH}$ is extracted from the parallel shift of $\ln(I_{\rm DS})$ versus $V_{\rm GS}$ in the subthreshold region, as mentioned in [19].

Comparisons of the threshold voltage versus effective channel length of the fully depleted SOI MOSFETs with

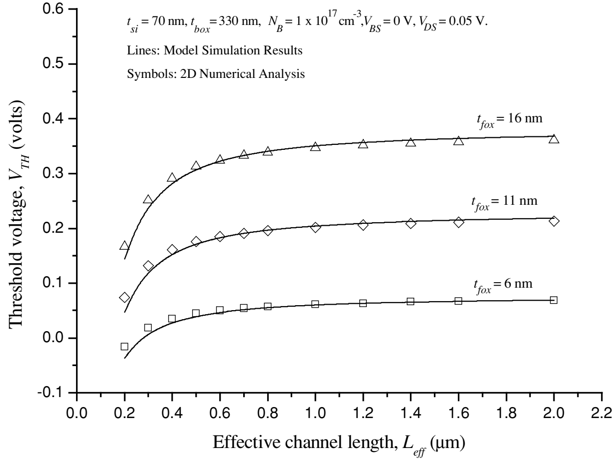

Figure 4. The calculated threshold voltage as a function of effective channel length with the thickness of the front gate oxide as a parameter.

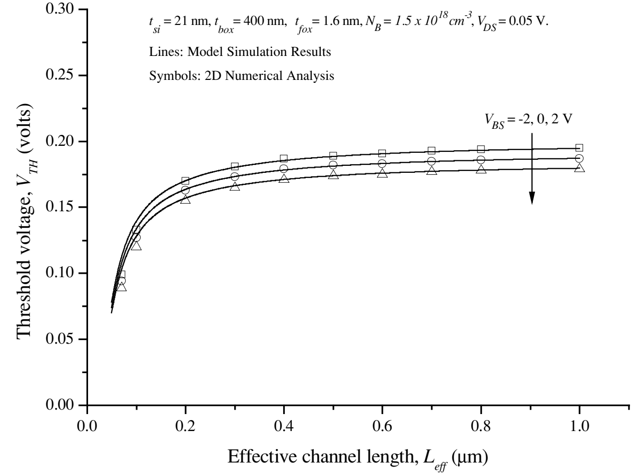

Figure 6. The calculated threshold voltage as a function of effective channel length with the back gate bias voltage as a parameter.

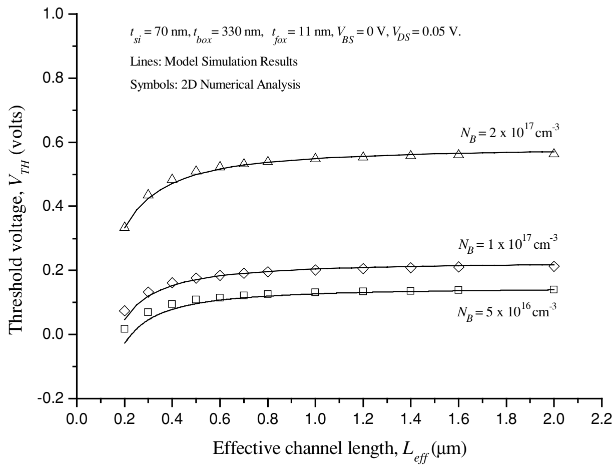

Figure 5. The calculated threshold voltage as a function of effective channel length with the doping concentration of the bulk Si film as a parameter.

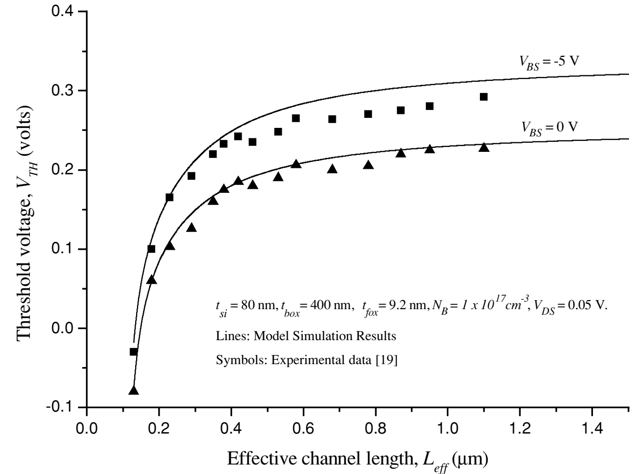

Figure 7. The threshold voltage roll-off versus effective channel length for different back gate biases from the present model and experiment.

11 nm front gate oxide, 330 nm buried oxide and 1×10^{17} cm^{-3} bulk doping concentration for different Si-film thicknesses are shown in figure 3 when $V_{\mathrm{DS}} = 0.05$ V and $V_{\mathrm{BS}} = 0$ V. In this figure, it is seen that the roll-off of the threshold voltage is more severe in the case of thicker Si film due to the short channel effect. In other words, the V_{TH} roll-off starts to occur at larger gate lengths in the MOS transistors with thicker Si films. Additionally, it is clearly seen that the calculated results using the present model agree very well with the 2D numerical analysis.

Figure 4 shows comparisons of the threshold voltage versus effective channel length for the devices of 70 nm Si film, 330 nm buried oxide and 1×10^{17} cm^{-3} bulk doping concentration with front gate oxide as the parameter. From this figure, it is seen that the devices with thinner front gate oxides can significantly retard the roll-off of the V_{TH} as the channel length gets shorter. This is because with thinner front gate oxide, the control ability of the gate over the depletion region under it becomes better. It is also seen that a good agreement is obtained between the simulated results and 2D numerical analysis. Figure 5 shows comparisons of the threshold voltages obtained by the proposed model with those extracted from 2D numerical analysis. From this figure, a satisfying agreement is obtained.

Figures 6 and 7 compare the roll-off of the threshold voltages for different back gate voltages with 2D numerical analysis and experimental data. As can be seen, the present model correctly predicts the V_{TH} roll-off for different back gate biases. Figure 8 shows the effect of the drain voltage on the roll-off of the threshold voltage of the devices with 1.6 nm front gate oxide, 400 nm buried oxide, 21 nm Si film and 1.5×10^{18} cm^{-3} bulk doping concentration. It is seen that at larger drain bias, the encroachment field from the drain becomes more significant, especially at small channel length. From this figure, accurate predictions of the severe threshold voltage roll-off by the proposed model are obtained, even for the devices with 0.07 μm channel length. Figure 9 shows comparisons of the threshold voltages obtained by

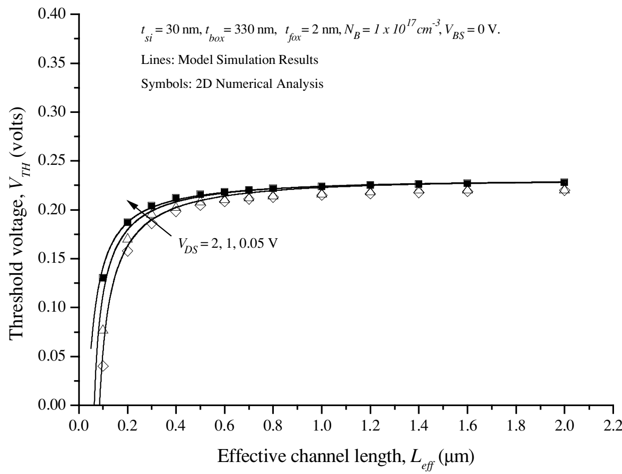

Figure 8. The calculated threshold voltage as a function of effective channel length with the drain bias voltage as a parameter.

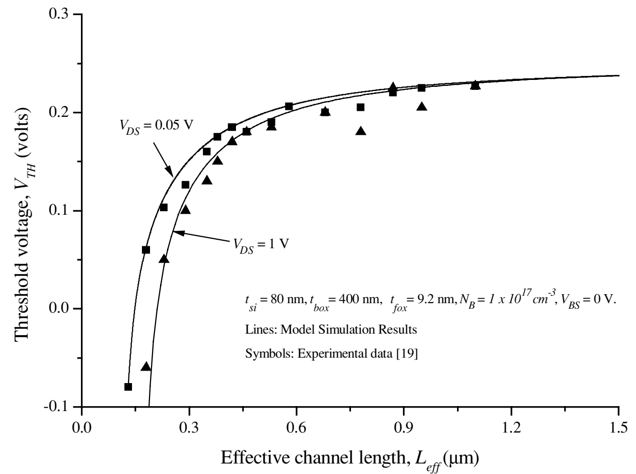

Figure 9. The threshold voltage roll-off versus effective channel length for different drain biases from the present model and experiment.

the present model with experimental data for the devices biased at different drain voltages. In this figure, it is seen that a good agreement is obtained between the simulated results and the experimental data. The present model is compared with the numerical data used in [16] (figures 5–7) and the compared results are shown in figure 10. From the figure, it is seen that a good agreement is obtained and it evaluates the validity of the modified model.

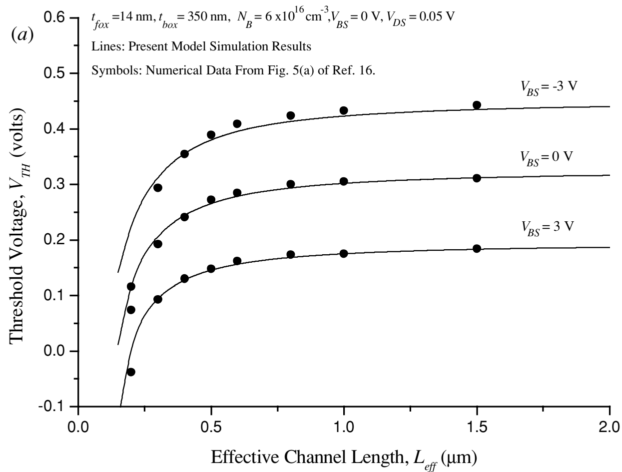

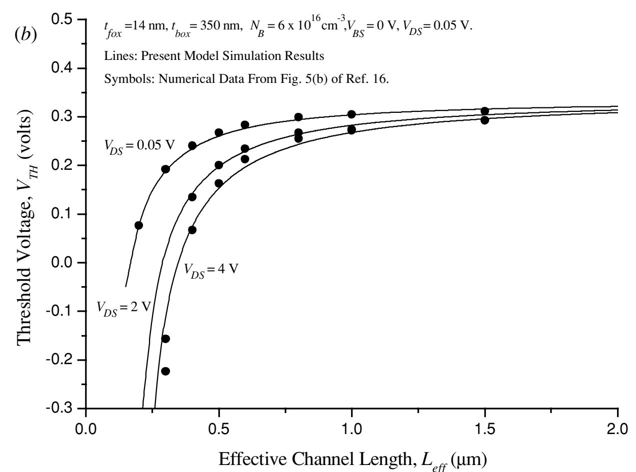

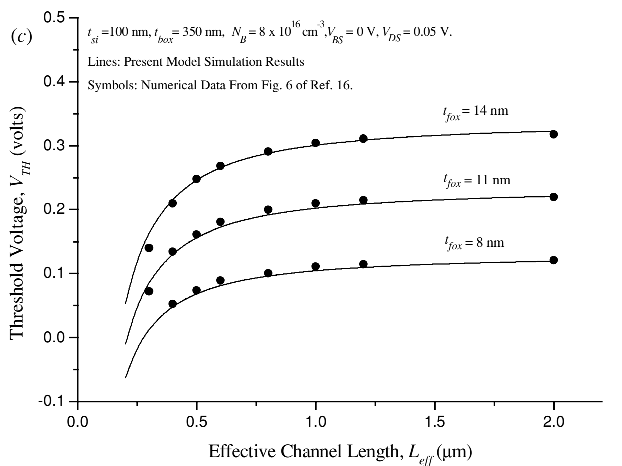

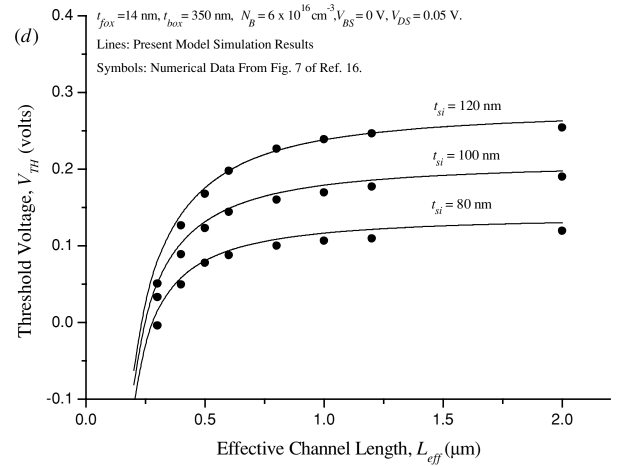

Figure 10. The calculated threshold voltage as a function of effective channel length with (*a*) V_{BS}, (*b*) V_{DS}, (*c*) t_{fox}, and (*d*) t_{si} as the parameters.

4. Conclusions

In this paper, we propose an analytical threshold voltage model for deep-submicrometre FD SOI MOSFETs using the three-zone Green's function technique to solve the 2D Poisson equation and adopting a new concept of the average electric field to avoid iterations in solving the position of the minimum surface potential. Firstly, we obtain the 2D potential distribution in the Si-film region by using the Green's function technique to solve the 2D Poisson equation. By applying Gauss's law at the Si–SiO_2 interface, the initial expression of the threshold voltage is obtained. Then, we introduce a modified factor to compensate for the errors resulting from the charge-sharing effect in the derivations of the final threshold voltage model. The proposed model is validated against the data obtained from 2D numerical analysis and experimental data and excellent agreements are obtained. From the above discussions, it can be seen that the present model predicts the threshold voltage well and has no iteration problem in the calculation that exists in the previous work [16].

Acknowledgments

The helpful suggestions and discussion with Dr C Y Wu and Dr J H Wang are gratefully acknowledged.

References

[1] Trivedi V P and Fossum J G 2003 *IEEE Trans. Electron Devices* **50** 2095
[2] Vandooren A *et al* 2002 *IEEE Int. SOI Conf.* **p 25**
[3] Zhang R and Roy K 2002 *IEEE Trans. Electron Devices* **49** 852
[4] Ohno T *et al* 1995 *IEEE Trans. Electron Devices* **42** 1481
[5] Doyle B S *et al* 2003 *IEEE Electron Device Lett.* **24** 263
[6] Luyken R J *et al* 2002 *IEEE Int. SOI Conf.* p 137
[7] Auberton A J *et al* 1995 *Semiconductor Int.* p 97
[8] Yoshimi M *et al* 1989 *IEEE Trans. Electron Devices* **36** 493
[9] Colinge J P 1989 *Int. Electron Devices Meeting Tech. Digest* p 817
[10] Joachim H O 1993 *IEEE Trans. Electron Devices* **40** 1812
[11] Colinge J P 1996 *Silicon-on-Insulator Technology: Materials to VLSI* (London: Kluwer)
[12] Ohno T *et al* 1987 *IEEE Circuits Devices Mag.* **3** 21
[13] Young K K 1989 *IEEE Trans. Electron Devices* **36** 399
[14] Veeraraghavan S and Fossum J G 1989 *IEEE Trans. Electron Devices* **36** 522
[15] Woo J C S *et al* 1990 *IEEE Trans. Electron Devices* **37** 1999
[16] Guo J Y and Wu C Y 1993 *IEEE Trans. Electron Devices* **40** 1653
[17] Jackson J D 1998 *Classical Electrodynamics* (New York: McGraw-Hill)
[18] MEDICI, V4.0 1998 *Tech. Rep.* Technology Modelling Associates, Inc., Palo Alto, CA
[19] Banna S R *et al* 1995 *IEEE Trans. Electron Devices* **42** 1949